

THE DEVELOPMENT OF A MAGNETO-OPTIC
CURRENT-MEASUREMENT SYSTEM
FOR HIGH, PULSED CURRENTS

by

H.S. Lassing

Rijnhuizen Report 85-161

THE DEVELOPMENT OF A MAGNETO-OPTIC CURRENT-MEASUREMENT SYSTEM
FOR HIGH, PULSED CURRENTS

by

H.S. Lassing
Association Euratom-FOM
FOM-Instituut voor Plasmafysica
Rijnhuizen, Nieuwegein, The Netherlands

ABSTRACT

In this paper a current-measurement system based on the Faraday rotation in a single-mode fiber is described. It is shown that an ultra low birefringence "spun" single-mode fiber is extremely suitable for use in a magneto-optic current-meter. The properties of this fiber have been investigated. Measurements of high, pulsed currents ($I_{\max} \sim 1$ MA; $f = 25$ kHz) with good accuracy and in accord with theory are presented. In order to calculate the current unambiguously and more accurate from the signals of the current-meter, a system with a double detector (to measure $\sin 2\vartheta$ and $\cos 2\vartheta$ simultaneously) was constructed. Measurements of high, pulsed currents with this system are also presented.

1. INTRODUCTION

1.1 Current measurements in SPICA II

SPICA II [1] is a 2.8 MJ screw-pinch experiment, which has started operation recently. A cross-sectional view is given in Fig. 1.1.

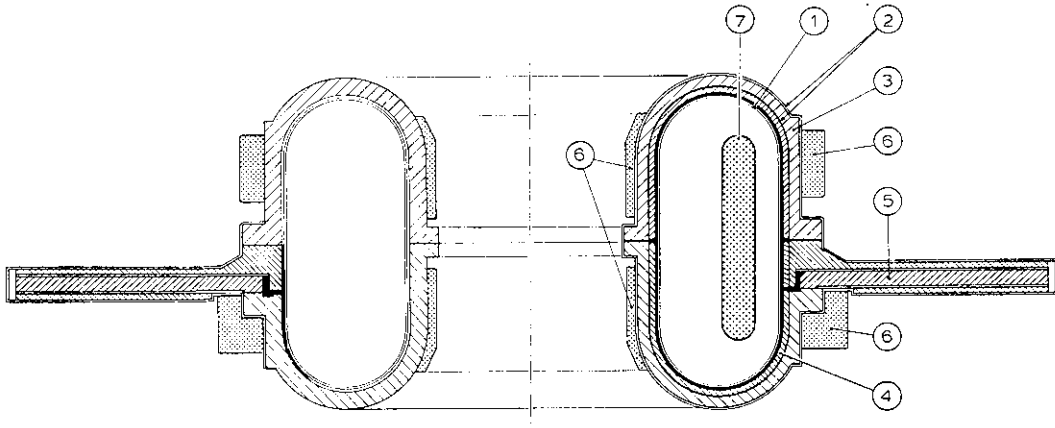


Fig. 1.1. Cross-sectional view of the SPICA II load assembly at the toroidal gap (right) and at an arbitrary position.

- | | |
|--|---|
| 1. Quartz vacuum vessel. | 4. Metal shield to screen the gap. |
| 2. Epoxy resin insulation. | 5. Feeding flange of the poloidal coil. |
| 3. Aluminum shell, also poloidal coil. | 6. Primary toroidal coils. |
| | 7. Plasma column. |

One of the basic parameters of a discharge in this experiment is the total electrical current carried by the plasma in toroidal direction. This plasma current, which has a peak value around 700 kA and a duration of about 1 ms, should be measured accurately and with a good time resolution ($\leq 1 \mu\text{s}$), especially during the first phase, in which the current changes rapidly. Figure 1.2 shows a typical example of the current as a function of time.

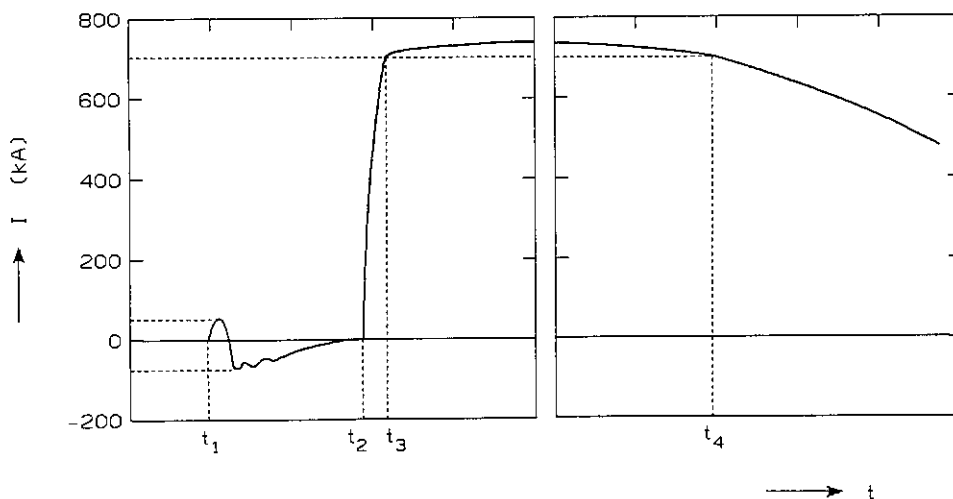


Fig. 1.2. Typical waveform of the expected plasma current in SPICA II.
 $t_1 = -100 \mu\text{s}$, $t_2 = 0$, $t_3 = 10 \mu\text{s}$, $t_4 = 1000 \mu\text{s}$.

The conventional instrument, a Rogowski coil, has in this particular case a number of disadvantages:

- The (conducting) coil must be insulated with respect to the metal shell.
- Near the gap in the shell a section of the Rogowski coil has to be omitted to prevent breakdown.
- The system is sensitive to electromagnetic interference.
- The integration of the output signal is difficult, because the current behaves almost like a step function.

To circumvent these problems a diagnostic has been developed based on the Faraday effect. This development was inspired by the review article of A.M. Smith [2].

1.2 The principle of the magneto-optic current measurement

The Faraday effect is a well-known optical phenomenon. If an external magnetic field H is applied to a suitable medium such that there is a field component parallel to the direction of propagation of the light, travelling through that medium, it is observed that the polarization state of the emergent light is changed. Especially if linearly polarized light is launched into the medium, it is found that the direction of polarization of the emergent light is rotated through an angle ϑ such that:

$$\vartheta = V \int_L \vec{H} \cdot d\vec{l},$$

where L is the path traversed by the light in the medium and V is the so-called Verdet constant, which depends on the medium and the wavelength of the light (V is proportional to λ^{-2}). For fused silica and at a wavelength of 633 nm, the Verdet constant is 4.68×10^{-6} rad/A [2,3].

It is attractive to use the Faraday effect in a fiber to measure a current, because the fiber can then be used as a light guide and as a transducer. The fiber is placed in a loop Γ around a conductor which carries a current. For the rotation of the plane of polarization we find, using Ampère's law:

$$\vartheta = V \int_{\Gamma} \vec{H} \cdot d\vec{l} = V \iint_A j_{||} dA = V \cdot I \quad (1.1)$$

with

J_n = component of the current density, normal to the plane of the loop,

A = area of the loop,

I = total current enclosed by the loop.

The rotation of the plane of polarization, ϑ , is measured by means of a Wollaston prism. The prism produces two orthogonal linearly polarized beams of light with small angular divergence. The intensities of the two beams are detected separately by photodiodes and the latter are connected to an analog electronic circuit, which computes the function $(I_1 - I_2)/(I_1 + I_2) = I$.

Assume the Wollaston prism is oriented such that with zero current all light falls upon one of the two photodiodes ($I = 1$). If a current I is flowing through the loop, then the fiber rotates the plane of polarization with $\vartheta = V.I$ with respect to the axis of the Wollaston prism, and the intensities seen by the photodiodes are in this particular case:

$$I_1 = C_1 (E_0 \sin\vartheta)^2 \text{ and } I_2 = C_2 (E_0 \cos\vartheta)^2 .$$

(E_0 = amplitude of the electric field vector of the light emerging from the fiber.)

If the photodiodes and the amplifiers are balanced, then $C_1 = C_2$ and:

$$I = \frac{I_1 - I_2}{I_1 + I_2} = - \cos 2\vartheta .$$

If the Wollaston prism (together with the photodiodes) is now rotated over 45 degrees, we find:

$$I = - \sin 2\vartheta . \tag{1.2}$$

Thus the quantity I gives us information about ϑ , whereas I does not depend on the intensity of the light emerging from the fiber. However, Eq. (1.2) is valid only if the fiber does preserve the state of polarization in the absence of the Faraday effect, and regardless the angle of polarization.

1.3 Demands on the optical fiber

There are several causes that can change the state of polarization of the light travelling through a fiber. In the first place, in multi-mode fibers, many propagation modes are possible. These modes have different velocities and hence, different phases when reaching the end of the fiber thus causing depolarization. In single-mode fibers only one propagation mode can exist, so no depolarization due to

different modes occurs. Impurities in the medium can also cause depolarization. The depolarization of the single-mode quartz fiber, used in our experiments, is negligible.

The one propagation mode in a single-mode fiber can still have all possible polarization states. These modes can therefore be described as a superposition of two independent polarized modes. When these two polarized modes have different propagation velocities, the state of polarization of the guided light is changed: this is called birefringence. There exist two types of birefringence; linear birefringence, if two orthogonal linearly polarized modes have different indices of refraction, and circular birefringence if a left-hand circularly polarized mode and a right-hand circularly polarized mode have different indices of refraction.

There are several mechanisms [4] producing birefringence. These mechanisms can be divided into intrinsic and external mechanisms. Intrinsic mechanisms are a non-circular cross-section of the core and asymmetrical lateral stress frozen into the fiber during manufacturing. External mechanisms are pressure, bending, electric field, twist and magnetic field. Twist and longitudinal magnetic field cause circular birefringence, the others lead to linear birefringence.

A fiber with very low linear birefringence must be used for correct current measurements. The fiber used in the experiments is a low birefringence fiber with circular core. The fiber has a permanent twist imparted to it by a spinning of the preform during fiber drawing and is therefore called a "spun" single mode fiber [5]. Electric fields have negligible influence on this fiber, because of the very small Kerr constant of quartz: 10^{-16} mV^{-2} [6]. If an electric field is applied perpendicular to the fiber, the linear birefringence δ_k caused by the Kerr effect is given by [7]:

$$\delta_k = j \cdot l \cdot E^2 ,$$

with j = Kerr constant; l = path length; E = electrical field strength. The maximum toroidal electrical field in SPICA II is approximately 10 kV m^{-1} ; the path length is about 2 m, so a maximum birefringence of only $\delta_k = 2 \times 10^{-8}$ rad is to be expected.

If the fiber is twisted the circular birefringence is small, unless the twist rate is very large [4]. The birefringence caused by other external mechanisms and the intrinsic birefringence of this fiber were examined (see Chapter 4).

In Chapter 2 the theory of plane polarized light which propagates through a fiber is reviewed. In Chapter 3 a description of the experimental setup is given. DC current measurements and determination of the Verdet constant are reported in Chapter 5. Chapter 6 deals with pulsed current measurements and in Chapter 7 efforts to measure simultaneously $\sin 2\vartheta$ and $\cos 2\vartheta$ (which is necessary if the current is to be calculated automatically) are described.

2. DESCRIPTION OF THE TRANSMISSION OF PLANE POLARIZED LIGHT THROUGH A FIBER

2.1 A method to measure linear birefringence of a fiber

The setup shown in Fig. 2.1 is used to measure linear birefringence:

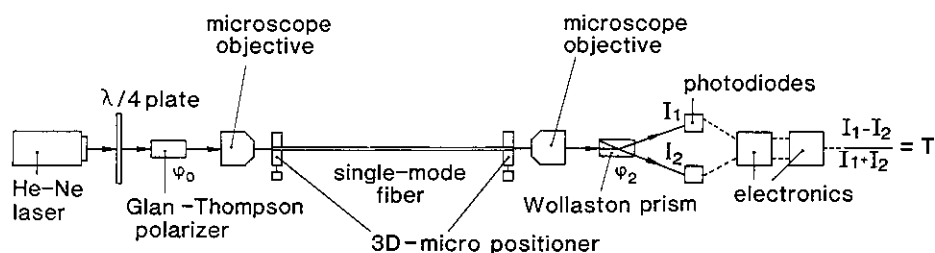


Fig. 2.1. Experimental setup for birefringence measurements.

The $\lambda/4$ plate near the laser is used to produce circularly polarized light. The polarizer can then be rotated, while the intensity of the emerging light remains constant.

The polarization state of the light can be described using Jones matrix calculation [8], if we assume the linear retarder model for the fiber [3]. This implies that the linear birefringence per unit length is a constant and also that the direction of linear birefringence is constant throughout the fiber.

We chose a rectangular coordinate system, with the x- and y-axes parallel to the axes of linear birefringence of the fiber, and the z-axis parallel to the length of the fiber.

The length of the path travelled by the light is z and the electric field-vector of the light is described by a plane wave equation:

$$E_z = E_0 e^{j(\omega t - kz)} .$$

If the polarizer is oriented with an angle ϕ_0 with respect to the x-axis the light launched into the fiber is characterized by:

$$\begin{pmatrix} E_x \\ E_y \end{pmatrix}_{z=z_1} = \begin{vmatrix} \cos \phi_0 \\ \sin \phi_0 \end{vmatrix} E_0 e^{j(\omega t - kz_1)} ,$$

with z_1 is the path travelled by the light.

At the end of the fiber there is a phase difference δ between x- and y-polarized waves so the electric field vector of the light coming out of the fiber is

$$\begin{pmatrix} E_x \\ E_y \end{pmatrix}_{z=z_2} = \begin{vmatrix} e^{j\delta/2} & 0 \\ 0 & e^{-j\delta/2} \end{vmatrix} \begin{vmatrix} \cos \phi_0 \\ \sin \phi_0 \end{vmatrix} E_0 e^{j(\omega t - kz_2)}$$

The Wollaston prism then splits the light beam into two light beams with orthogonal polarizations. If the angle of the Wollaston is ϕ_2 with respect to the x-axis, the amplitudes of the electric field vector of the light falling upon the photodiodes is calculated with:

$$\begin{pmatrix} E_1 \\ E_2 \end{pmatrix}_{z=z_3} = \begin{vmatrix} \cos \phi_2 & \sin \phi_2 \\ -\sin \phi_2 & \cos \phi_2 \end{vmatrix} \begin{vmatrix} e^{j\delta/2} & 0 \\ 0 & e^{-j\delta/2} \end{vmatrix} \begin{vmatrix} \cos \phi_0 \\ \sin \phi_0 \end{vmatrix} E_0 e^{j(\omega t - kz_3)}$$

For the final result of the electronics, I , it is then found:

$$I = \frac{|E_1|^2 - |E_2|^2}{|E_1|^2 + |E_2|^2} = \cos 2\phi_2 \cos 2\phi_0 + \sin 2\phi_2 \sin 2\phi_0 \cos \delta$$

The linear birefringence is determined as follows: for different values of ϕ_0 (the angle of the polarizer), the detector (ϕ_2) is rotated such, that I has its maximum value. If $\phi_0 = 0^\circ$ (this is with respect to the x-axis or the y-axis) then the maximum of I will be 1. If $\phi_0 = 45^\circ$, then the maximum will be $\cos \delta$.

If the measured values of the maximum of I are plotted versus ϕ_0 the minimum value of I gives us $\cos \delta$. Figure 2.2 shows an example.

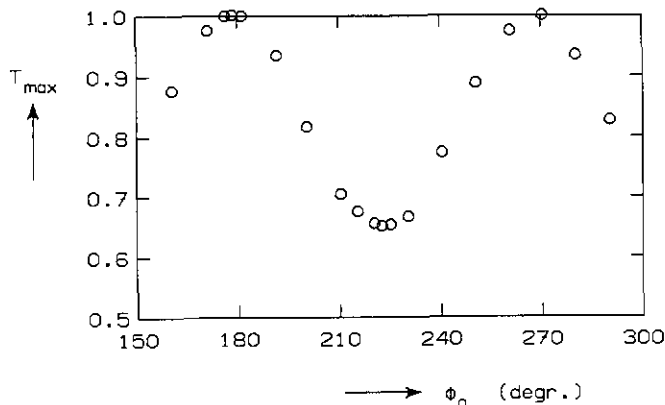


Fig. 2.2. Maximum value of I , plotted versus ϕ_0 . ϕ_0 is measured with respect to an arbitrary direction.

2.2 The measurement of a small linear birefringence

The method described in Sec. 2.1 for measurements on the linear birefringence gives us $\cos \delta$, and is therefore not very accurate, when δ is close to zero. The light emerging from the fiber is somewhat elliptically polarized, because of the linear birefringence. With the detector the "degree of polarization" is measured, assuming the light is linearly polarized and this results in $\cos \delta$.

In order to achieve a more sensitive measurement, for small δ , a $\lambda/4$ plate is inserted just before the Wollaston prism and it is adjusted to produce circularly polarized light out of linearly polarized light [9].

The electric field vector of the light that falls on the photodiodes 1 and 2 is calculated as follows:

$$\begin{pmatrix} E_1 \\ E_2 \end{pmatrix} = \begin{vmatrix} \cos\phi_2 & \sin\phi_2 \\ -\sin\phi_2 & \cos\phi_2 \end{vmatrix} \begin{vmatrix} 1+j\cos 2\phi_1 & j\sin 2\phi_1 \\ j\sin 2\phi_1 & 1-j\cos 2\phi_1 \end{vmatrix} \begin{vmatrix} e^{j\delta/2} & 0 \\ 0 & e^{-j\delta/2} \end{vmatrix} \begin{vmatrix} \cos\phi_0 \\ \sin\phi_0 \end{vmatrix} E_0 e^{j\omega t},$$

with ϕ_1 = angle of the quarter wave plate.

Calculation of the signal I leads to:

$$I = \frac{|E_1|^2 - |E_2|^2}{|E_1|^2 + |E_2|^2} = \cos 2(\phi_1 - \phi_2) \{ \cos 2\phi_0 \cos 2\phi_1 + \sin 2\phi_0 \sin 2\phi_1 \cos \delta \} + \sin 2(\phi_1 - \phi_2) \sin 2\phi_0 \sin \delta.$$

If the $\lambda/4$ plate and the detector are rotated such that $\phi_1 - \phi_2 = \pi/4$ rad then $I = \sin 2\phi_0 \sin \delta$.

In this case I is independent of the absolute value of ϕ_1 or ϕ_2 . The detector now only sees circularly polarized light. When the polarizer (ϕ_0) is rotated till a maximum of the quantity I is obtained then this maximum will be equal to $\sin \delta$. This "sine-method" should be used when a small birefringence has to be measured, because a better accuracy can be reached.

2.3 The optical signal of the current-meter if a fiber with linear birefringence is used

The setup which is used for current measurements is shown in Fig. 2.3.

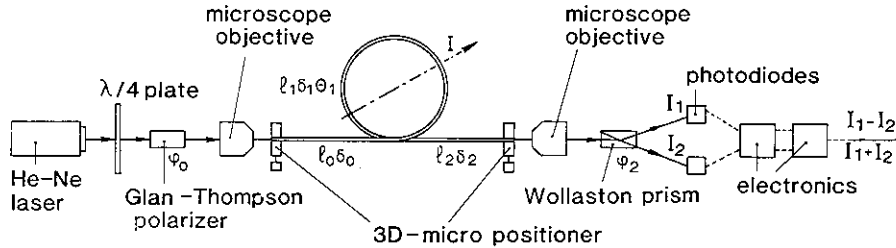


Fig. 2.3. Experimental setup for current measurements.

Coming from the laser, the light passes successively through: a $\lambda/4$ -plate, a polarizer at an angle of ϕ_0 , a fiber section with length ℓ_0 and linear birefringence δ_0 , the fiber loop with length ℓ_1 , linear birefringence δ_1 and circular birefringence ϑ_1 (due to the Faraday rotation), a fiber section with length ℓ_2 and linear birefringence δ_2 , and finally the Wollaston prism with the two photodiodes at an angle ϕ_2 .

The problem of a medium having both linear and circular birefringence is treated by W.J. Tabor and F.S. Chen [10] by means of the Jones-matrix calculation. This was used by A.M. Smith [3] to calculate the signal I of a setup similar to the setup of Fig. 2.3.

In order to simplify this analysis the input polarization is chosen to be parallel to one of the axes of linear birefringence:

$$\begin{pmatrix} E_x \\ E_y \\ 0 \end{pmatrix} = \begin{bmatrix} 0 \\ E_0 e^{j\omega t} \end{bmatrix}.$$

This means that if no current is passing through the fiber loop, the light emerging from the fiber is still completely linearly polarized in the initial direction.

Furthermore the detector is rotated in such a way that it detects the two directions of polarization corresponding to

$$E_1 = \frac{E_x + E_y}{\sqrt{2}} \text{ and } E_2 = \frac{E_x - E_y}{\sqrt{2}} .$$

This means that with zero current, I equals zero.

With these adjustments, it follows that [3]:

$$I = - 2\cos(\delta_2 + \eta)\sin\chi \sin(\phi/2) \{ \cos^2(\phi/2) + \cos^2\chi \sin^2(\phi/2) \}^{1/2} \quad (2.1)$$

with:

$$\begin{aligned} (\phi/2)^2 &= (\delta_1/2)^2 + \vartheta_1^2, \\ \tan \chi &= 2 \vartheta_1 / \delta_1, \\ \eta &= \tan^{-1} (\cos\chi \tan(\phi/2)). \end{aligned}$$

In the first part of the fiber the direction of polarization is parallel to an axis of birefringence, so δ_0 does not show up in the formula for I .

Figure 2.4 (See [12]) gives a plot of I versus ϑ_1 for different values of δ_1 and δ_2 . When δ_1 and δ_2 are both equal to zero, Eq. 2.1 reduces to $I = - \sin 2\vartheta_1$.

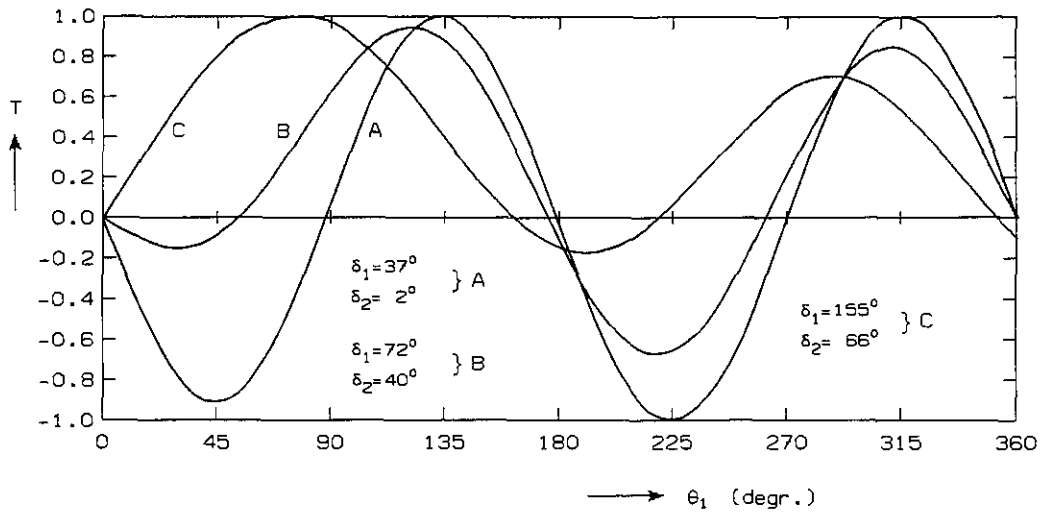


Fig. 2.4. Plots of I versus ϑ_1 for different values of δ_1 and δ_2 .

2.4 Current measurement with a "cosine detector"

The setup shown in Fig. 2.3 can also be used to measure $\cos 2\theta$. To realize this, the detector must be rotated such that I equals 1, when the current is zero. Then each photodiode sees one of the two independently polarized modes: $E_1 = E_x$, $E_2 = E_y$. The equation for the electric field vector at the end of the fiber remains unchanged (See [3]):

$$\begin{pmatrix} E_x \\ E_y \end{pmatrix} = \begin{vmatrix} -BE_0 \exp(j[\omega t + \delta_2/2]) \\ |A|E_0 \exp(j[\omega t - \delta_2/2 - \eta]) \end{vmatrix}$$

with $A = \cos(\phi/2) + j \cos \chi \sin(\phi/2)$

$B = \sin \chi \sin(\phi/2)$

χ and $\phi/2$ see Eq. 2.1

For the signal I it now follows:

$$I = -\cos 2\chi \sin^2(\phi/2) - \cos^2(\phi/2) \tag{2.2}$$

Since each photodiode sees one of the two polarized modes a phase shift between the two modes is not seen, and therefore δ_2 does not occur in Eq. 2.2.

When $\delta_1 = 0^\circ$, Eq. 2.2 reduces to $I = -\cos 2\theta_1$.

3. EXPERIMENTAL APPARATUS

The magneto-optic current-meter consists of three parts:

- the lightsource,
- the fiber,
- the detecting part.

3.1 The lightsource

The lightsource consists of the following components (see Fig. 3.1):

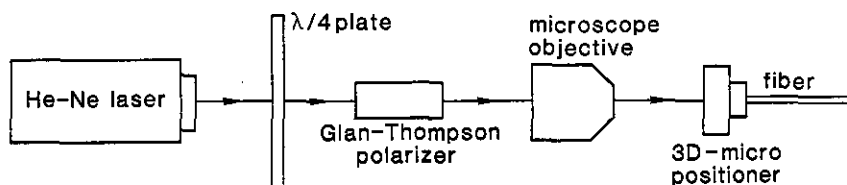


Fig. 3.1 The lightsource of the current-meter.

- a 5 mW He-Ne laser (wavelength 632.8 nm). Divergence of the beam is 1.0 mrad. The laser produces linearly polarized light.
- a quarter wave plate, rotated such that the light leaving the quarter wave plate is circularly polarized.
- a Glan-Thompson polarizer. The degree of polarization of the light that leaves the polarizer, is better than 99.5 %.
- a 20 x microscope objective. With this objective an image of the laser beam is made on the end-face of the fiber. Because of the beam divergence and the distance between microscope objective and fiber (5 mm), the spot of the laserbeam on the fiber has a diameter in the order of 5 μm , the same order of magnitude as the diameter of the core of the fiber.
- a 3D-micropositioner, to position the fiber-end in or near the focus of the microscope objective.

The possibility of using a laserdiode as a lightsource has been investigated. The most suitable wavelength available is 850 nm, which reduces the Verdet constant, and therefore the Faraday rotation ϑ , by

about a factor two, compared to the He-Ne laser light. An advantage of a laserdiode is, that the fiber can be fixed onto the laserdiode (pig-tail). This means that the light is launched into the fiber without adjustments and therefore the setup is less sensitive to mechanical vibrations. However, the direction of polarization is also fixed. It can be made adjustable with the help of a single-mode connector and a weld. In this way a setup with a laserdiode would not be simpler than a setup with a He-Ne laser. Also a laserdiode is easily destroyed by moderate interference on the powersupply lines. Therefore, it is not very simple to use a laserdiode in the SPICA II experiment. As a consequence the use of a laserdiode has been abandoned.

3.2 The fiber

As stated in Sec. 1.3, the fiber is a "spun" single-mode fiber, type LB600 manufactured by York V.S.O.P., consisting of a core (diameter $5\ \mu\text{m}$) and a cladding (diameter $100\ \mu\text{m}$). The fiber is single-mode for a wavelength of $633\ \text{nm}$. The fiber is equipped with a silicon coating with a twofold function:

- the fiber is mechanically much stronger than a fiber without coating (diameter coating is $300\ \mu\text{m}$);
- the cladding modes are stripped by the coating, because the index of refraction of the coating is higher than that of the cladding.

The ends of the fiber are fixed in a rectangular groove (width $0.3\ \text{mm}$) of a brass cylinder in order to avoid pressure on the fiber. Furthermore, the fiber is led through a teflon tube ($2\ \text{mm}$ O.D.) also to avoid pressure on the fiber.

3.3 The detecting part

The detecting part of the experimental setup consists of the following components (Fig. 3.2):

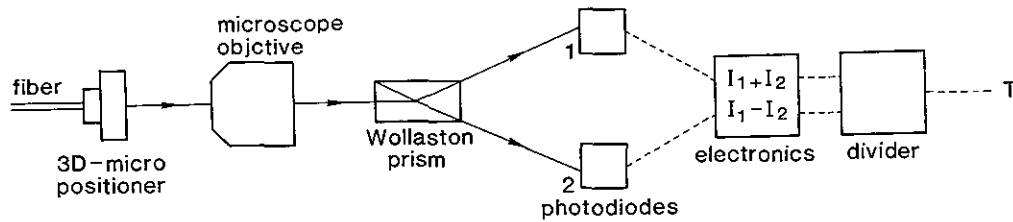


Fig. 3.2. The detecting part of the current-meter.

- a 3D-micropositioner.
- a 20 x microscope objective, used to focus the emerging light onto the photodiodes. The cone of the light emerging from the fiber is the same as the cone of the light launched into the fiber. A parallel beam can be made with the microscope objective. However since the active surface of the photodiodes is only 5 mm^2 it is preferable to focus the lightbeam onto the photodiodes.
- a Wollaston prism, angle of divergence 20 degrees,
- two PIN photodiodes, which measure the intensities I_1 and I_2 ,
- analog electronics, to form the signals $I_1 - I_2$ and $I_1 + I_2$ (adder/subtractor),
- an analog divider with output $T = (I_1 - I_2)/(I_1 + I_2)$.

The Wollaston prism, the two photodiodes and the adder/subtractor are all fixed onto a rotatable disc; this whole is denoted as the detector. The read-out accuracy of the angle of the rotatable disc is about 15 minutes $\approx 4 \times 10^{-3}$ rad.

4. PROPERTIES OF THE FIBER, USED IN THE EXPERIMENTS

4.1 Introduction

The fiber appeared to be very strong (mechanically) and the cladding modes were not observed, because of the silicon coating.

Circular birefringence was measured a few times and it was not greater than 20 degrees. Circular birefringence only causes an offset of the zero line and changes nothing in the results of the current measurements.

The intrinsic linear birefringence of the fiber was measured, and also the linear birefringence due to external mechanisms.

4.2 Intrinsic linear birefringence (δ_i)

The linear birefringence of pieces of the fiber with various lengths was measured with the methods described in Secs. 2.1 and 2.2. During the experiments, the fiber is lying on a horizontal plane. A very small force on the fiber keeps it in a straight line.

Table 4.1 shows the results. Some remarks on these results: The measured linear birefringence consists of an intrinsic part and an unknown contribution due to external mechanisms (pressure, bending, etc). In particular the ends of the fiber are kept in a rectangular groove by means of a thin sheet of metal with the same width as the groove. In order to keep the fiber in contact with the bottom of the groove, inevitable some pressure must be applied to the fiber. Because of the small width (0.3 mm) a certain force (for example 0.5 N) on the metal sheet, already leads to a considerable pressure (length groove = 5 cm, $p = 3.3 \times 10^4$ Pa) and this will lead to a birefringence with the same order of magnitude as the measured birefringence (about 14 degrees). Furthermore, the pressure induced birefringence will be different for each measurement. Therefore:

- the measured birefringence is not equal to the intrinsic birefringence;
- it is certain that the intrinsic birefringence is not greater than the values listed in Table 4.1

Table 4.1

length of fiber (m)	measured linear birefringence (degrees)	
	sine method (sec 2.1)	cosine method (sec (2.2))
0.25	5	4
0.44	8	5
0.98	7	6
1.56	12	12
1.80	12	14
1.90	12	12

The difference between the results of the methods of Secs. 2.1 and 2.2 is due to the $\lambda/4$ plate, which was not very accurate.

4.3 Linear birefringence due to external mechanisms

4.3.1 Pressure

The fiber was placed in a circular groove, with a length $l = 60$ mm, in an aluminum plate. On top of the fiber another aluminum plate was placed plus a number of weights. See Fig. 4.1.

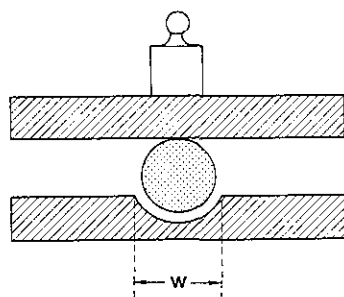


Fig. 4.1. Various pressures were applied in this way to the fiber.

If the total weight on the fiber is denoted by F , then the pressure p on the fiber is approximately given by:

$$p = F/A, \text{ with } A = l.w, \quad w = 0.28 \text{ mm.}$$

For different values of the pressure, the linear birefringence (δ_m) was measured, and the linear birefringence due to the pressure per meter fiber (δ_p) was calculated after a correction for the intrinsic birefringence (δ_i) as follows:

$$\delta_p = (\delta_m - \delta_i)/l, \quad \text{with } l = 60 \text{ mm.}$$

The results are shown in Fig. 4.2.

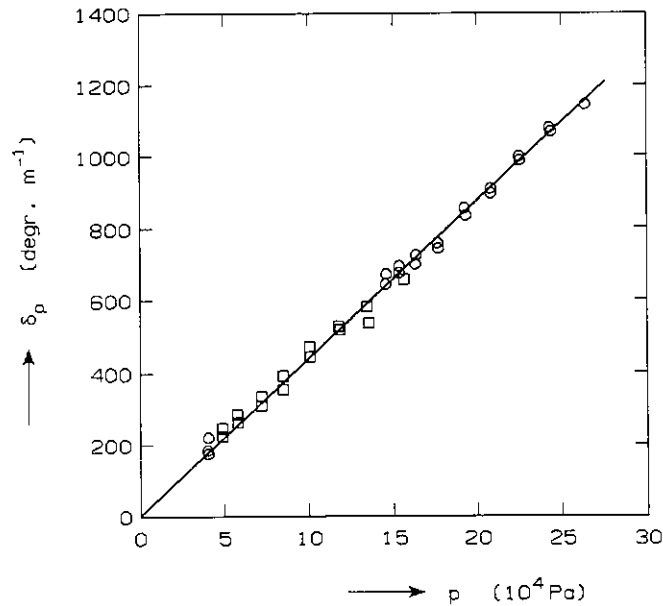


Fig. 4.2. The linear birefringence, caused by the pressure, per meter fiber, (δ_p) measured as a function of pressure p .

Since δ_p is proportional to the pressure, one can derive a constant:

$$\delta_p/p = 7.4 \times 10^{-5} \text{ rad.m.N}^{-1}.$$

This value is 200 times smaller than the value found elsewhere [3]. This difference in result may be due to the silicon coating.

4.3.2. Bending

To measure the effect of bending, the fiber is wound twice around cylinders with several radii (r). A small force is applied along the fiber in order to keep it in touch with the surface of the cylinder, and to keep the beginning and the end of the fiber in a straight line. From these measurements, the linear birefringence due to bending, per meter fiber (δ_b) is calculated from the measured linear birefringence with:

$$\delta_b = (\delta_m - \delta_i)/l \quad \text{with } l = 4 \pi r, \text{ the length of the bent fiber.}$$

The results are shown in Fig. 4.3.

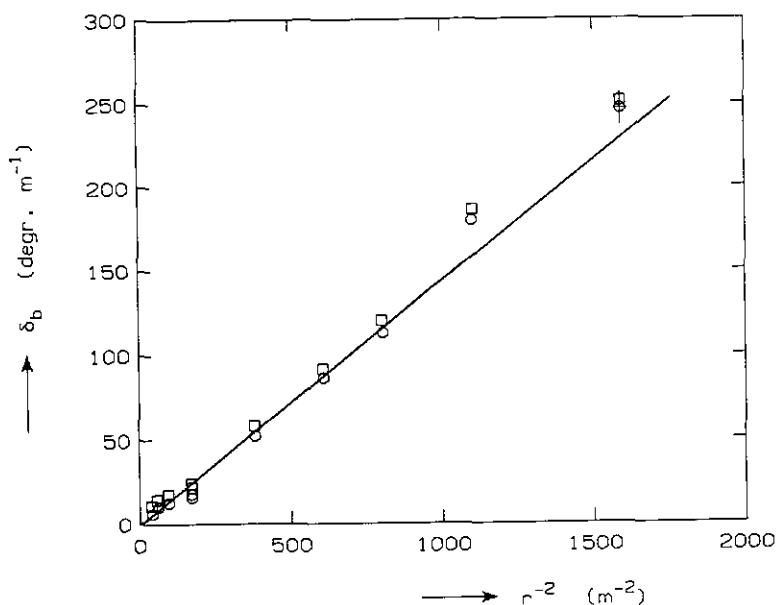


Fig. 4.3. The linear birefringence, caused by the bending of the fiber per meter fiber, (δ_b), measured as a function of the bending radius (r).

In agreement with results reported elsewhere [4,11] the bending-induced birefringence is proportional to r^{-2} .

4.3.3. Mechanical vibrations

In order to examine the effect of mechanical vibrations on the fiber, the fiber is attached to the cone of a loudspeaker, which is vibrating with frequencies of 10 - 10^4 Hz. A significant effect is only measured, when simultaneously a pressure is applied to the fiber.

4.4 Conclusion

The intrinsic linear birefringence of the fiber is low enough to be neglected.

The birefringence induced by bending the fiber is in the particular case of SPICA II (with a bending radius of 15 cm) only 5° and thus also small enough as will be discussed in Sec. 5.5 and Sec. 6.2.3. One should however carefully avoid any pressure onto the fiber along its entire length because this leads to a considerable birefringence.

As a conclusion it can be said that the spun single-mode fiber is quite suitable for use in a magneto-optic current-meter.

5. CALIBRATION

5.1 Introduction

In a magneto-optic current-meter the current is calculated from $I = \vartheta/V$, so the Verdet constant should be known. To measure the Verdet constant of the fiber, a D.C.-current setup was constructed, so that for different values of I , both ϑ and I could be measured.

5.2 The D.C.-current experimental setup

The D.C.-current experimental setup consists of the following parts (see Fig. 5.1):

- a current source (40 V, 15 A),
- a conventional current-meter, consisting of a shunt of 10.3 m Ω and a voltmeter (100 mV, 2 mA),
- three identical coils with 712 turns each, connected in series,
- the magneto-optic current-meter. The fiber is passing through the three coils, thus enclosing 2136 turns.

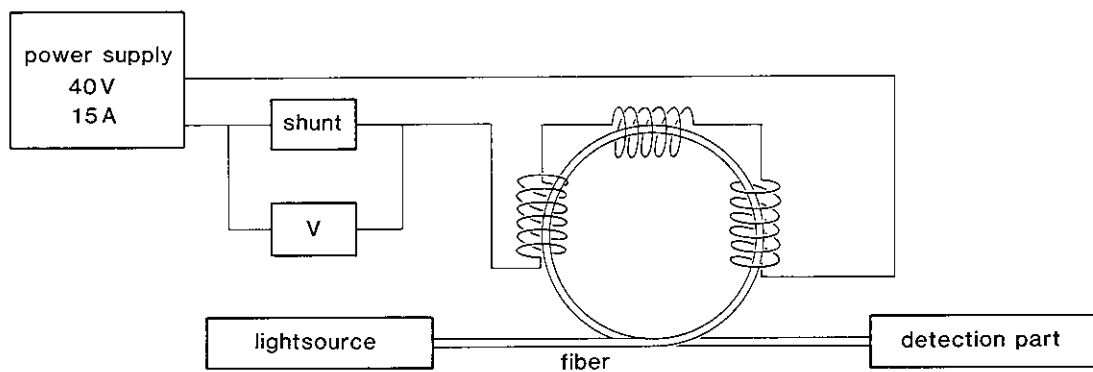


Fig. 5.1. Experimental setup for D.C.-current measurements.

The bending radius of the fiber is 15 cm. The linear birefringence of the fiber in this setup was measured to be:

$$\delta = \delta_0 + \delta_1 + \delta_2 = (12 \pm 0.5) \text{ degrees.}$$

5.3 The adjustment of the current-meter

Before this setup can function properly as a current-meter, some adjustments have to be made. First to minimize the effect of the birefringence, the direction of polarization of the light launched into the fiber, must be adjusted parallel to an axis of birefringence. This is affected by rotating the polarizer into a proper position. After this, the detector is rotated, until I equals zero, which means that the detector now forms an angle of $\pi/4$ radians with an axis of birefringence of the fiber.

When these adjustments are made, and the birefringence is small, it then follows:

$$I = -\sin 2\vartheta \text{ (see Sec. 2.3)}$$

It is not possible to make I equal to zero exactly, in practice $|I| < 0.001$. This corresponds with a rotation of the detector of 1 mrad. The error in the current resulting from this inaccuracy is about 100 A.

5.4 Results

The maximum current through the coils was 7.27 A. The fiber then enclosed 15.5 kA turns. During the measurement, the optical signal I and the current I were registered simultaneously. The results are plotted in Fig. 5.2. Since the rotation of the plane of polarization was only 4.1 degrees at the maximum current, the diagram represents a straight line ($|I| = \sin 2\vartheta = 2V \cdot I$, for $\vartheta \ll \pi/4$ rad).

After returning to zero current, the optical signal was changed by 1.7×10^{-3} corresponding to a current of 0.2 kA. This is caused by drift in the electronic circuit, as can be seen from Fig. 5.2, which shows a slightly different slope for increasing and decreasing currents (total time for ramping the current up and down was 20 minutes). From the mean slope, the Verdet constant was calculated:

$$V = (4.60 \pm 0.02) \times 10^{-6} \text{ rad/A} \quad (5.1)$$

For this calculation of V , no correction was made for the linear birefringence.

5.5 Discussion

The value found for the Verdet constant, Eq. 5.1, can be compared to the Verdet constant for fused silica: $V = 4.68 \times 10^{-6}$ rad/A [3] and the value found by A.M. Smith [3] for a somewhat different type of fiber: $V = 4.54 \times 10^{-6}$ rad/A.

Further calculations were made with Eq. (2.1) (Sec. 2.3), with $\delta_1 = \delta_2 = 0^\circ$ and with $\delta_1 = 5^\circ$; $\delta_2 = 3.5^\circ$ (Table 5.1). From this table it is seen that there is no need to take the linear birefringence into account, when V is calculated.

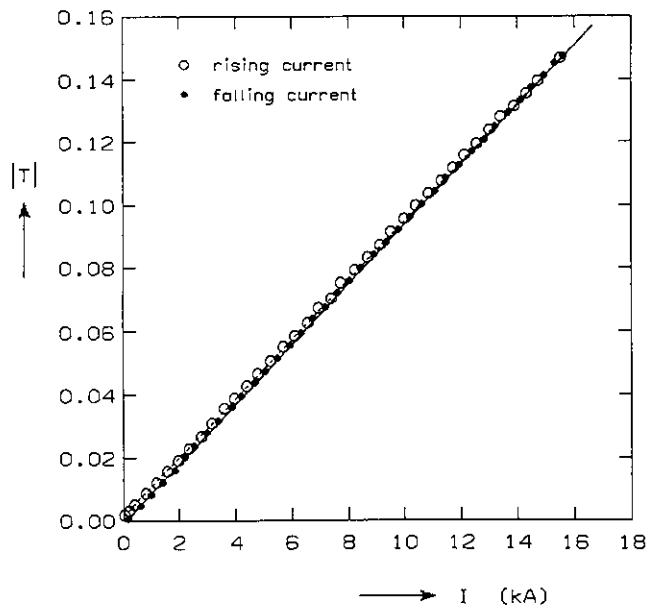


Fig. 5.2. Signal I measured as a function of the effective current I .

TABLE 5.1

Calculation of T with $V = 4.6 \times 10^{-6}$ rad/A

δ_1 (degrees)		0	5	10	
δ_2 (degrees)		0	3.5	5	
I kA	δ_1		T	T	T
	degrees	rad			
0.034	0.01	0.000	-0.0003	-0.0003	-0.0003
1.922	0.51	0.009	-0.0176	-0.0175	-0.0173
2.777	0.73	0.013	-0.0255	-0.0253	-0.0251
3.845	1.01	0.018	-0.0353	-0.0351	-0.0347
5.084	1.34	0.023	-0.0467	-0.0464	-0.0459
5.724	1.51	0.026	-0.0526	-0.0523	-0.0517
6.408	1.69	0.029	-0.0589	-0.0585	-0.0579
7.220	1.90	0.033	-0.0663	-0.0659	-0.0652
8.800	2.32	0.040	-0.0808	-0.0804	-0.0795
9.890	2.61	0.045	-0.0908	-0.0903	-0.0893
10.640	2.80	0.049	-0.0977	-0.0971	-0.0961
11.340	2.99	0.052	-0.1041	-0.1035	-0.1024
12.070	3.18	0.056	-0.1108	-0.1101	-0.1089
12.880	3.39	0.059	-0.1182	-0.1175	-0.1162
13.840	3.65	0.064	-0.1269	-0.1262	-0.1248
15.170	4.00	0.070	-0.1391	-0.1383	-0.1368

6. PULSED CURRENT MEASUREMENTS

6.1 Description of the experimental setup

6.1.1 The model

In the SPICA-II experiment the fiber encircles the minor cross-section of the toroidal vacuum vessel once. A cross-sectional view of the vessel and the surrounding current-carrying shield is given in Fig. 6.1.

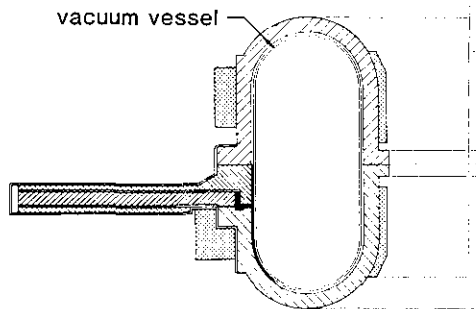
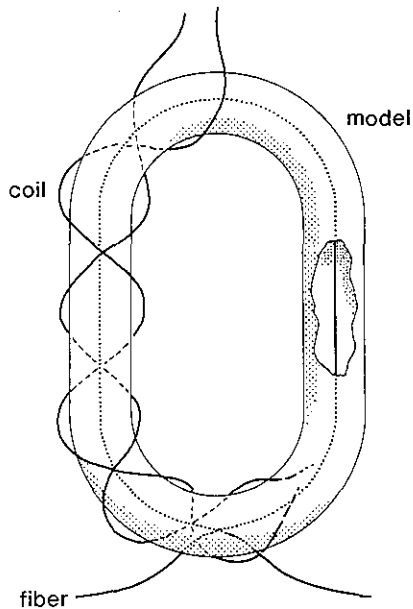


Fig. 6.1. Cross-section of the vacuum vessel and the surrounding current-carrying shield of SPICA II.



To create the same geometry for the fiber, a model with the same cross-section was constructed. This model, also used to support the coil for the current, is shown in Fig. 6.2.

Fig. 6.2. The model with the fiber and a part of the coil.

The coil consists of 18 wires. Nine wires are wound as a right-handed helix with n turns around the minor circumference and one turn around the major circumference of the model. The second set of nine wires are wound similarly but then as a left-handed helix. All wires are connected in parallel to the capacitor bank. Consequently, the net effect of all wire currents is a fairly smoothly distributed current around the minor circumference of the model (see Fig. 6.3).

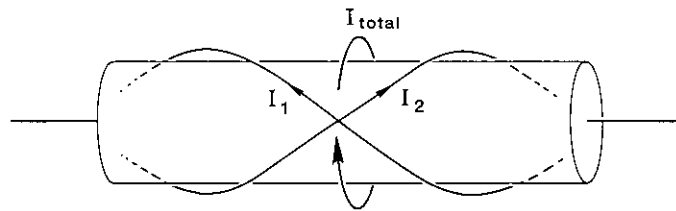


Fig. 6.3. The wires are connected to the capacitor such that the total current flows around the minor circumference.

Clearly, this configuration produces only toroidal flux so that it can be regarded as a single coil with n turns.

The self-inductance of an ideal toroidal coil of this type is:

$$L = \frac{\mu_0 A n^2}{\ell} ,$$

with ℓ = length of center-line of the toroid

A = area of the cross-section of the toroid

n = number of turns around the minor circumference.

Substituting $L = 1.35 \mu\text{H}$ (see Sec. 6.1.2), $\ell = 1.74 \text{ m}$ and $A = 5 \times 10^{-3} \text{ m}^2$ it is found that n must be 19. This means that each wire should have 19 turns around the minor circumference.

6.1.2 The current source

In order to reach about the same conditions for the current as in the SPICA-II experiment (risetime = 10 μs ; $I_{\text{max}} \approx 700 \text{ kA}$) we use four parallel capacitors, with a total capacity of $C = 31.2 \mu\text{F}$.

The capacitors can be charged up to $V_0 = 18$ kV and can be discharged over a coil with a sparkgap as a switch. This produces a damped harmonic oscillation of the current I , with:

$$I = I_{\max} e^{(j\omega t - t/\tau)}; \quad I_{\max} = \omega C V_0; \quad \omega = (LC)^{-1/2}; \quad \tau = 1/e\text{-time.}$$

Since the frequency should be 25 kHz, it follows that:

$$L = 1.35 \mu\text{H} \tag{6.1}$$

The coil consists of 19 turns, so that the maximum current to be produced is $700 \text{ kA} : 19 \approx 37 \text{ kA}$. This will be the case for $V_0 = 8 \text{ kV}$. The voltage on the capacitors is measured with an electrostatic voltmeter.

6.1.3 Miscellaneous equipment

The measurements of the optical system can be compared with those of a conventional Rogowski coil. The e.m.f. of the Rogowski coil is proportional to dI/dt . The signal was integrated by a passive integrator with an RC-time of 8.2 ms. (See Fig. 6.4.) The integrated signal was calibrated by extrapolation of the maxima and minima to $t = 0$ s, to obtain $I_{\max} = \omega C V_0$.

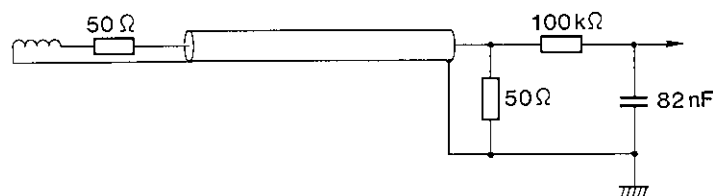


Fig. 6.4. The Rogowski coil and the integrator.

The analog electronics which computes the functions $I_1 - I_2$ and $I_1 + I_2$ had to be rebuilt for these pulsed current measurements. This was necessary because of the fast changes in the $I_1 - I_2$ signal (see Fig. 6.5). Since $I = -\sin 2\vartheta$ and $\vartheta = V.I = V.I_0 \sin \omega t$ the frequency of I is not a constant. The maximum frequency we observed was about 200 kHz.

PIN-photodiodes with build-in amplifiers (MDA 435) and fast operational amplifiers for adding and subtracting (HA 5195) were used. (See appendix Fig. A1.) The circuit is shielded by a metal box.

The signals of the Rogowski coil and the detected optical signals were measured with a wideband oscilloscope (Tektronix 7844) or a transient recorder (Biomation 8100). The latter two were placed inside a small screened room.

The polarizer and the detector are rotated to a suitable position in the same way as described in Sec. 5.3 .

6.2 Results

6.2.1 Current and optical signal versus time

Figure 6.5 shows an example of $I = (I_1 - I_2) / (I_1 + I_2)$ and the (integrated) Rogowski signal versus time. Both signals are recorded simultaneously with the two-channel transient recorder. The charging voltage of the capacitors was 9.0 kV. The period of the oscillation is determined from Fig. 6.5:

$$\tau = (44.5 \pm 0.5) \mu\text{s}.$$

At the first maximum ($t = 11 \mu\text{s}$) the current was calculated both from the Rogowski signal ($I = (713 \pm 7) \text{ kA}$) and from I ($I = (712 \pm 5) \text{ kA}$), and the two values agreed well.

The plane of polarization is seen to rotate over more than 180 degrees. Since $I = -\sin 2\vartheta$, one sees more than a complete period in the first 11 μs . In the next 11 μs I returns in the same way to zero. Figure 6.5 shows that the amplifiers and the divider receive a signal with a frequency of almost 200 kHz whereas the integrator of the Rogowski signal only deals with a signal of 20 kHz.

6.2.2 Exponential decay and accuracy

From Fig. 6.5 the maxima and minima of the current are calculated from both the Rogowski signal and the magneto-optical signal. The current is calculated from the magneto-optical signal according to the formulas:

$$I = -\sin 2\vartheta$$

$$I = \vartheta/V$$

with $V = 4.6 \times 10^{-6} \text{ rad/A}$ (from Sec. 5.4).

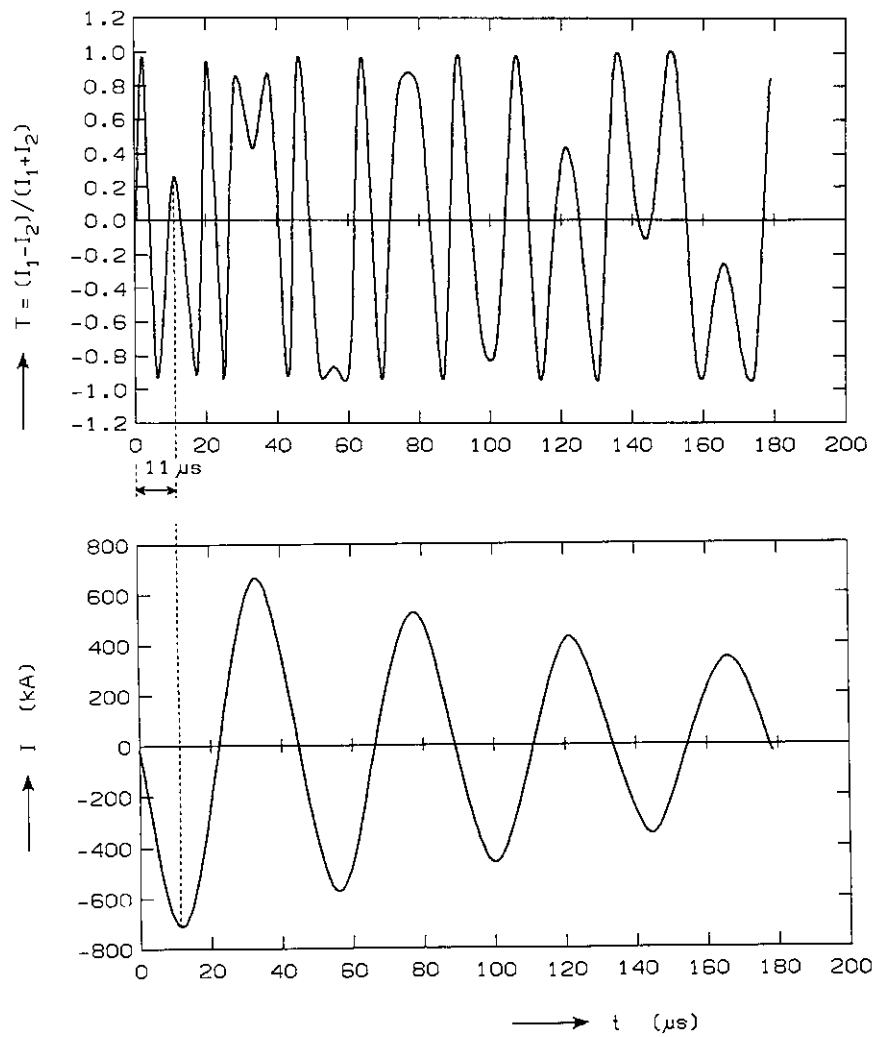


Fig. 6.5. The current (measured with the Rogowski coil) and the signal I from the magneto-optic current sensor, recorded simultaneously in a 9.0 kV shot.

Deviations between Rogowski and optical signal are less than 3% (see Table 6.1). The inaccuracy of the Rogowski signal is 1%, originating from the extrapolation by the calibration, and read-out errors. The inaccuracy of the optical signal is about the same, but when the plane of polarization is rotated more than 160° ($I > 600$ kA) the accuracy is better (0.5%). In that situation the current is calculated as follows (Fig. 6.6):

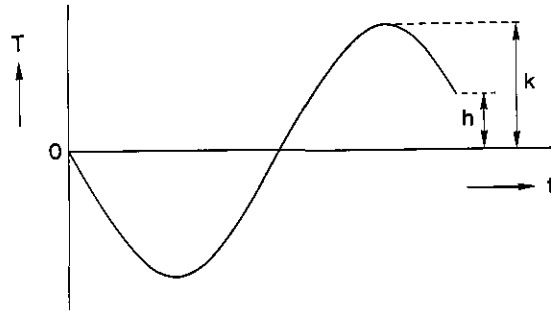


Fig. 6.6. The read-out of I at a moment t . The current is calculated from $I = \vartheta/V$, and $2\vartheta = 2\pi + \arcsin -h/|k|$.

The relative accuracy of 2ϑ is therefore better than the relative accuracy of $\arcsin -h/|k|$. When the rotation ϑ is about 135° and 45° (= 510 and 170 kA resp.) the accuracy of the optical signal is less, because $I = -\sin 2\vartheta$ is not very sensitive to changes in ϑ around these values of ϑ .

The maxima and minima of the current, calculated from the magneto-optical signal are plotted on a logarithmic scale (Fig. 6.7). Because of the exponential decay of the damped oscillation, this plot results in a straight line. For the straight line in Fig. 6.7 the equation:

$$I = 750 \exp(-t/192)$$

holds (t in μs ; I in kA). Deviations between this formula and the values obtained from the optical signal are not greater than 0.6% except for the data points at 512 kA and 457 kA (see Table 6.1). The rotation is then about 135° , which causes a reduced accuracy. The accuracy of this measurement can be increased if $\cos 2\vartheta$ is measured at the same time (see Sec. 7).

The value for $I_{\text{eff max.}}$ obtained from Fig. 6.7 (750 kA) is in good agreement with the value obtained by

$$I_{\text{eff max.}} = 19 \omega CV_0 = 752 \text{ kA.}$$

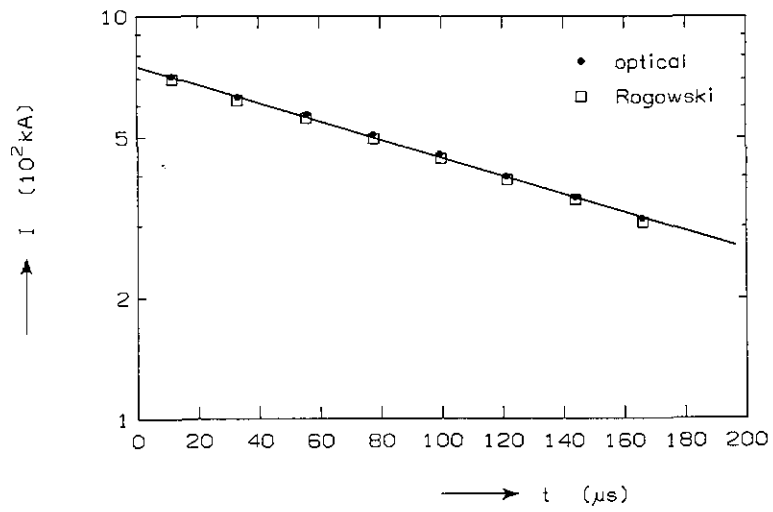


Fig. 6.7. The maxima and minima of the current (calculated from both signals) plotted logarithmically versus time.

TABLE 6.1

time (μ s)	current (kA)				
	measured		$\frac{I_r - I_o}{I_o}$	calculated= I_c	$\frac{I_o - I_c}{I_o}$
	I_o =optical	I_r =Rogowski	%		%
11	712	713	0.1	708	0.6
33	629 \pm 5	634	0.8	632	-0.5
56	559	574	2.7	560	-0.2
78	512	514	0.4	500	2.4
100	457	458	0.2	446	2.5
122	398	403	1.3	397	0.3
144	355	363	2.2	354	0.3
166	315	318	5.0	316	-0.3

6.2.3 Optical signal versus Rogowski signal (x-y plots)

A measurement was also done at a capacitor voltage of 15 kV, thus producing $I_{eff} \approx 1.2$ MA, with better time resolution (timebase 20.5 μ s long). At the top of the current the rotation was about 310° . A plot is shown in Fig. 6.8, upper part. At this time resolution, only 1 channel of the transient recorder, can be used, so the shot was repeated to register the Rogowski signal (Fig. 6.8, lower part).

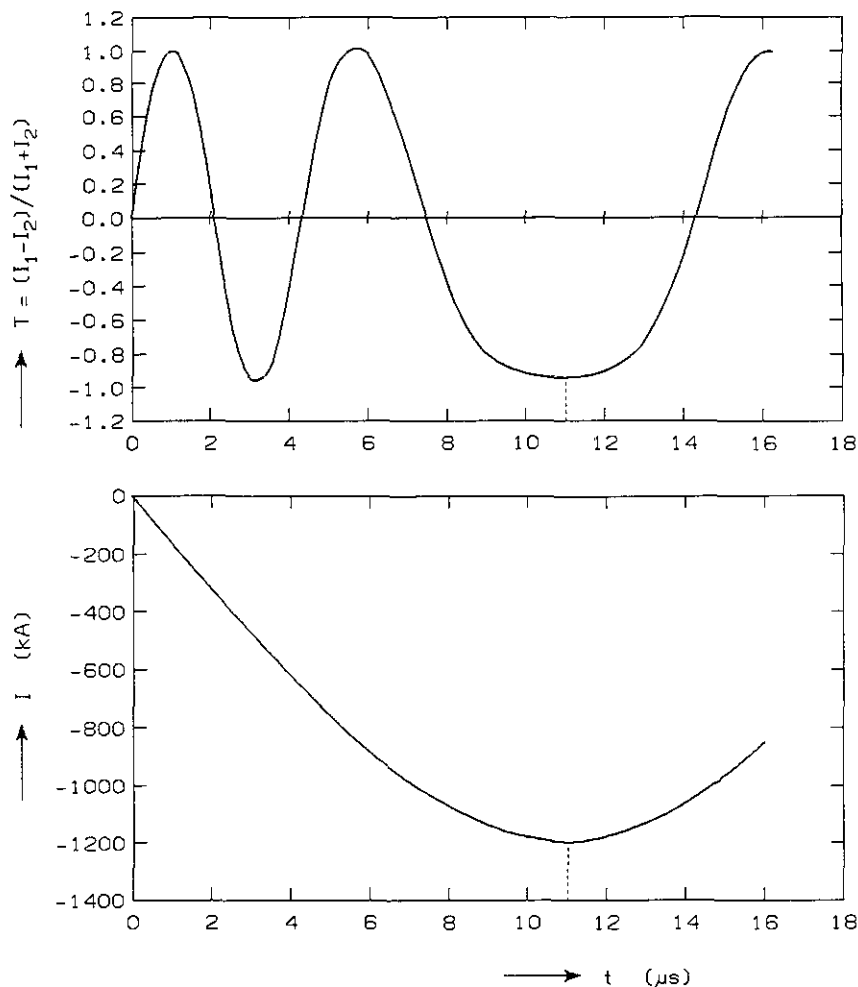


Fig. 6.8. Rogowski signal and T from a 15 kV shot.

From the Rogowski signal, the current is calculated as a function of time. The optical signal was then plotted as a function of the current (Fig. 6.9).

In this plot also $T = -\sin 2\phi$ (solid line) and Eq. (2.1) of Sec. 2.3 with $\delta_1 = 10^\circ$ and $\delta_2 = 5^\circ$ (dashed line) are shown.

The dashed line shows that when the fiber exhibits linear birefringence the first maximum of the current does not reach 1.0. Since this is not observed, linear birefringence of the fiber must be small. Thus in calculating the expected optical signal it is not necessary to take the linear birefringence into account.

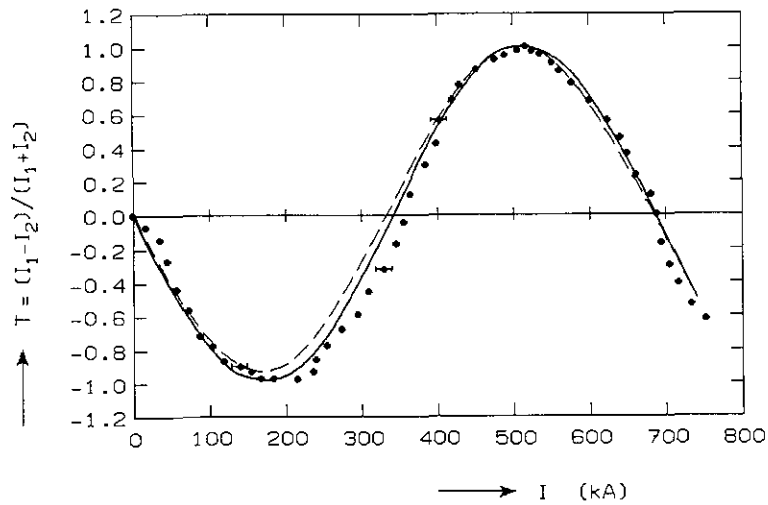


Fig. 6.9. T plotted versus the current I . The values were obtained from Fig. 6.8. Dots: measurement Fig. 6.8; solid line: $T = -\sin 2\theta$; dashed line: Eq. 2.1 with $\delta_1 = 10^\circ$ and $\delta_2 = 5^\circ$.

The deviation between measurements and theory is due to the inaccuracy in Rogowski signal (which is about 5% because of the small signal and the inaccuracy of the zero-line), the inaccuracy in the optical signal and because the plot is composed of data from two different shots. The optical signal can also be plotted directly versus the current in an oscilloscope x-y plot, as is shown in Fig. 6.10. The maximum effective current was 720 kA.

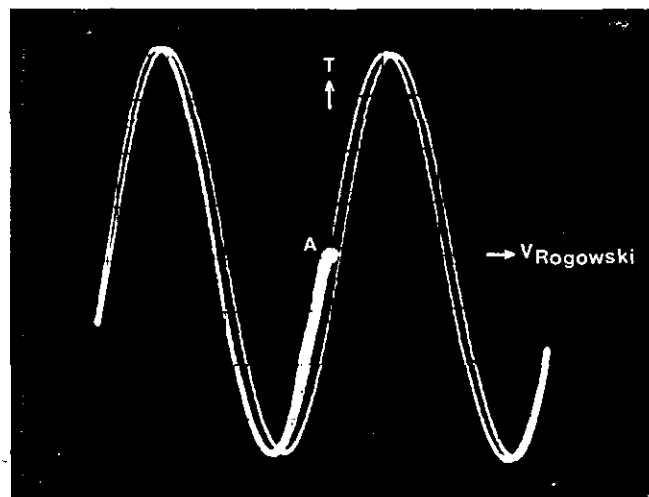


Fig. 6.10. Optical signal (T) plotted directly versus the Rogowski signal on an oscilloscope. "A" corresponds to $t = 0$, both signals growing negative in the first microseconds.

It is expected that the two lines coincide. Due to a small phase-shift in the divider, the two lines do not coincide completely. In a new magneto-optic current-meter (now under construction) a divider with a better frequency response will be used.

6.3 Discussion

Pulsed currents up to 1.2 MA (turns) were measured with the magneto-optic current-meter. The relative accuracy is at least as good as the accuracy of the Rogowski-coil. The accuracy becomes better everytime I passes a maximum (or minimum). Very close near a maximum (or minimum) the accuracy is somewhat less.

The linear birefringence of the fiber was low, so that no corrections for it had to be made in calculating the current. For proper measurement of currents of 1 MA max and with a frequency of 25 kHz, the analog electronics (including the divider) must have a flat frequency response and no phase shift up to 200 kHz.

7. DOUBLE DETECTOR MEASUREMENTS

7.1 Introduction

In the following it is assumed that $I = \sin 2\vartheta$ instead of $I = -\sin 2\vartheta$ (detector rotated over 180°).

The current cannot be directly obtained from the signal I , but has to be calculated as follows from the equations $I = \sin 2\vartheta$ and $I = \vartheta/V$:

$$I \text{ equals either } \frac{\arcsin I + n \cdot 2\pi}{2V} \text{ or } \frac{\pi - \arcsin I + n \cdot 2\pi}{2V}$$

with $n = 0, -1, 1, -2, 2, \dots$

This means that I is not uniquely determined by I , but one needs to know also n and whether $\arcsin I$ or $(\pi - \arcsin I)$ has to be used. This problem is absent in the special case that the current increases linearly with time from zero at $t = 0$. Then in the various regions shown in Fig. 7.1, I can be calculated as follows:

A: $I = \frac{\arcsin I}{2V}$

B: $I = \frac{\pi - \arcsin I}{2V}$

C: $I = \frac{2\pi + \arcsin I}{2V}$

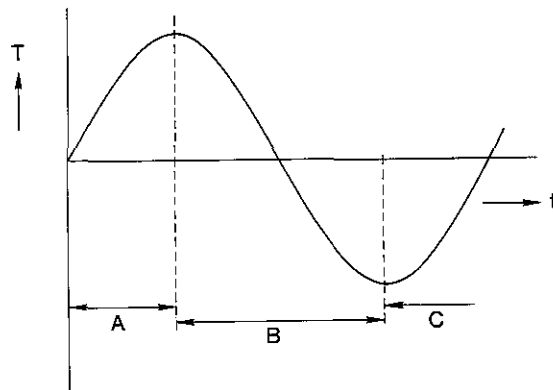


Fig. 7.1. The signal I , if the current increases linearly with time from zero at $t = 0$.

More generally, the current I can be derived unambiguously from I , whenever I changes monotonically with t , for example in the first quarter period of a sine wave. However, a problem arises when the general behaviour of the current is unknown; near a maximum or a minimum of I , it cannot be ascertained whether the current increases or decreases. (It may have changed from increasing to decreasing just in the maximum (or minimum.) A second problem is the accuracy of the current when $\vartheta = \pi/4, 3\pi/4, 5\pi/4, \dots$ radians. For small values of ΔI the possible error in I is:

$$\Delta I \approx \frac{\partial I}{\partial I} \cdot \Delta I = \{2V \sqrt{(1-I^2)}\}^{-1} \cdot \Delta I.$$

From this it can be seen that when $I \rightarrow 1$, ΔI is becoming very large. For larger values of ΔI , the possible error in I cannot become larger than $\Delta I_{\max} = I(I \pm \Delta I) - I(I) = 1/2V \{\arcsin(I \pm \Delta I) - \arcsin(I)\}$. An example, when $\Delta I = 0,01$ (read-out error) then $\Delta I/I$ can become 10% when $I = 1$, see Table 7.1.

TABLE 7.1

I	$\Delta I/I$	$\arcsin I$	I	$\Delta I/I$
0.50 ± 0.01	2 %	0.52 ± 0.01	57 ± 1	2 %
0.90 ± 0.01	1 %	1.12 ± 0.02	121 ± 3	2 %
0.98 ± 0.01	1 %	1.37 ± 0.06	149 ± 6	4 %
0.99 ± 0.01	1 %	1.43 ± 0.14	155 ± 15	10 %

I is calculated with $V = 4.6 \times 10^{-6}$ rad. A^{-1} .

Both problems are avoided if we measure $\sin 2\vartheta$ and $\cos 2\vartheta$ simultaneously, by splitting the light beam into two light beams and using two detectors, one rotated over $\pi/4$ radians with respect to the other.

When $\vartheta = \pi/8$ radians, $\sin 2\vartheta = \cos 2\vartheta = 0.707$. When ϑ rises above $\pi/8$ radians it is better to calculate I from $I^* = \cos 2\vartheta$: when ϑ is falling below $\pi/8$ radians, I is better calculated from $I = \sin 2\vartheta$. In this way the most accurate value is always obtained, and it is always clear whether the current is rising or falling (Fig. 7.2).

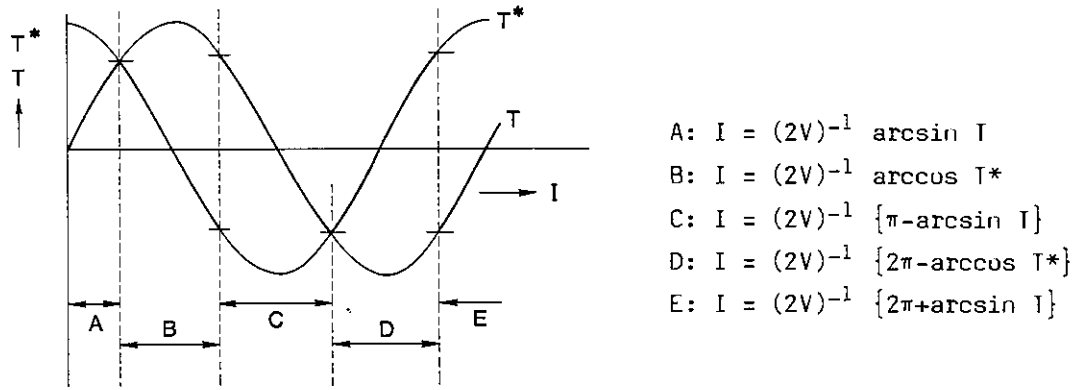


Fig. 7.2. $\sin 2\vartheta (=T)$ and $\cos 2\vartheta (=T^*)$ plotted simultaneously versus the current.

To decide which equation has to be used a computer program can be applied. An experimental setup to measure $\sin 2\vartheta$ and $\cos 2\vartheta$ simultaneously was constructed and some experiments were carried out.

7.2 Experimental setup

The following changes were made in the setup, described earlier in Chapter 3. In the detecting part of the setup a beamsplitter prism is placed between the microscope objective and the Wollaston prism. A second detector, consisting of a Wollaston prism, two PIN photodiodes and analog electronics, which computes the functions $I_1 - I_2$ and $I_1 + I_2$, all attached to a rotatable disk, has been built. It is placed in the reflected lightbeam such that the distance from the beamsplitter prism to the Wollaston prism is equal for both detectors (Fig. 7.3). All components, that is the two detectors, the beamsplitter, the microscope objective and the micropositioner, are firmly attached to a frame.

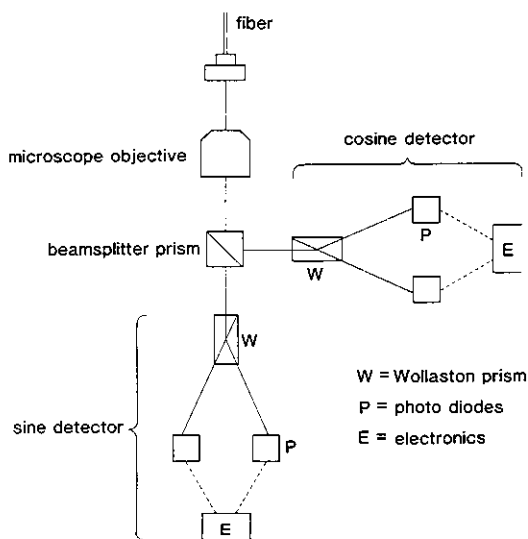


Fig. 7.3. Experimental setup for double detector measurements.

To position the reflected light beam into the middle of the Wollaston prism the beamsplitter prism can be rotated and inclined, to move the light beam in two independent orthogonal directions. The other light beam, to the first detector, is hardly influenced by these small adjustments.

The second detector is tuned differently from the first detector. Whereas the first detector is rotated until $I = 0$ (sine-detector) the second detector is rotated until $I = 1$ (or -1) at zero current (cosine-detector). In practice the detector is rotated until I has a maximum, which is hardly ever exactly 1.

7.3 Results

7.3.1 Optical signal versus time

There are two ways to register the signals coming from the sine- and the cosine-detector simultaneously. One is to use two dividers, and register $I = (I_1 - I_2) / (I_1 + I_2)$ from both detectors.

Alternatively one could register $I_1 - I_2$ and $I_1 + I_2$ from both detectors. Then four signals need to be recorded simultaneously; $I = (I_1 - I_2) / (I_1 + I_2)$ can be calculated afterwards.

Since only one divider and one two-channel transient recorder were available the measurements could not be made according to either one of the two methods described.

With the setup described in Chapter 6 also $I_1 - I_2$ and $I_1 + I_2$ are recorded simultaneously. The result is shown in Fig. 7.4.

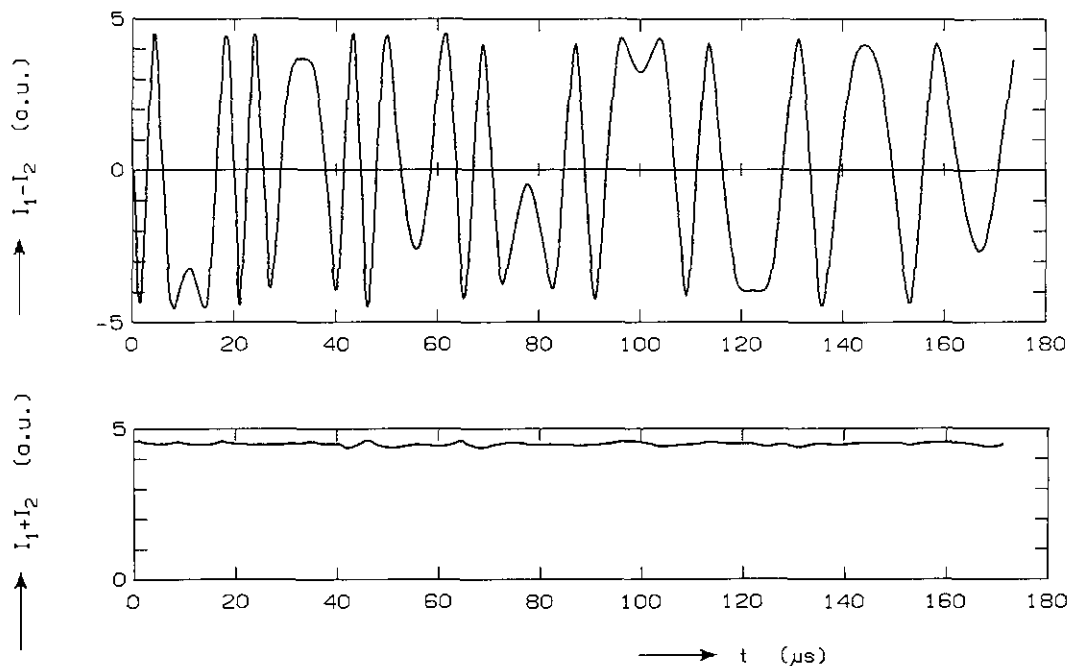


Fig. 7.4. $I_1 - I_2$ and $I_1 + I_2$ measured without beamsplitter ($I = \sin 2\vartheta$).

Since I_1+I_2 is almost a straight line, I_1-I_2 must have a shape similar to $(I_1-I_2)/(I_1+I_2) = T$.

Therefore the best solution with the double detector seemed to be to record just I_1-I_2 from both detectors. This was carried out and the result is shown in Fig. 7.5.

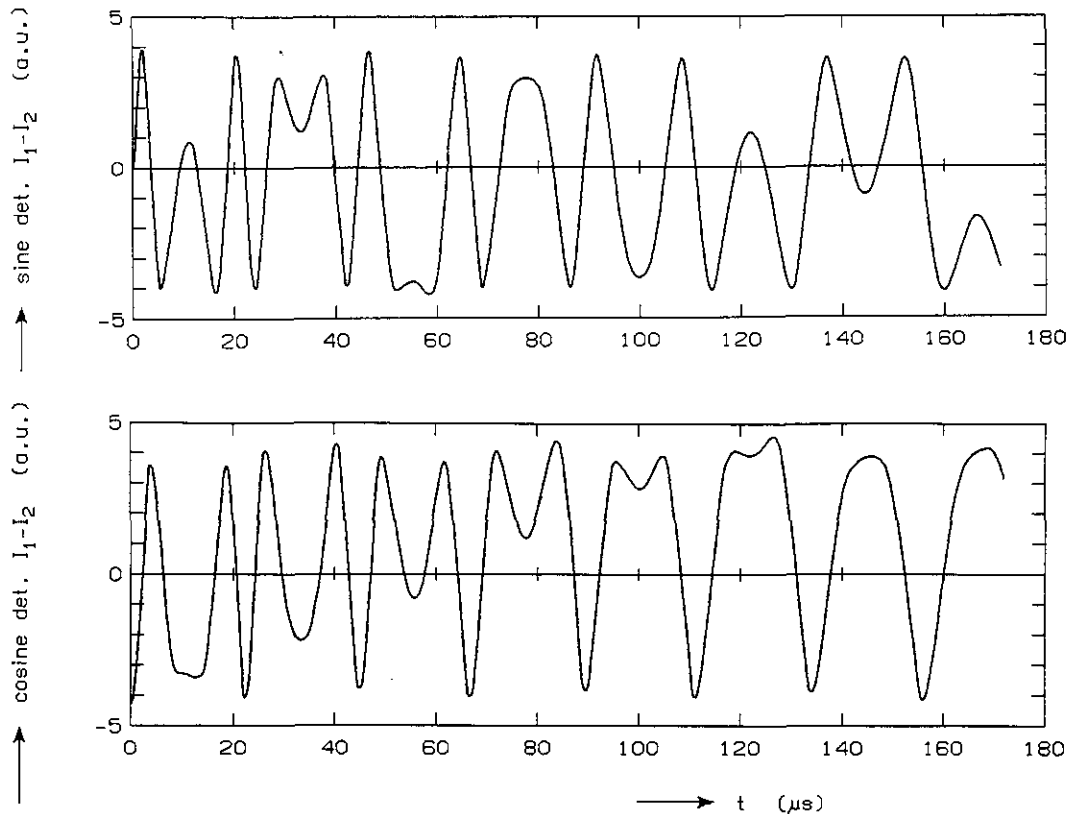


Fig. 7.5. I_1-I_2 measured simultaneously with both sine- and cosine- detector. ($V_0 = 9.0$ kV, $I_{\max} = 710$ kA).

7.3.2 Exponential decay; accuracy

As described in Sec. 6.2.2 the accuracy of a measurement can be studied from a log-linear plot of the maxima and the minima of the current versus time. For the result of Fig. 7.5 this is done in Fig. 7.6. It is obvious that the measurement is not very accurate.

This inaccuracy is caused by the fact that the two I_1+I_2 signals are not constant in this case. As a consequence I_1-I_2 will certainly not have a shape similar to $T = (I_1-I_2)/(I_1+I_2)$. Figure 7.7 shows a plot of both I_1+I_2 and I_1-I_2 from the cosine detector, versus time. It turns out that the deviation of I_1+I_2 from a constant is due to the polarization properties of the beamsplitter prism (see Sec. 7.3.3).

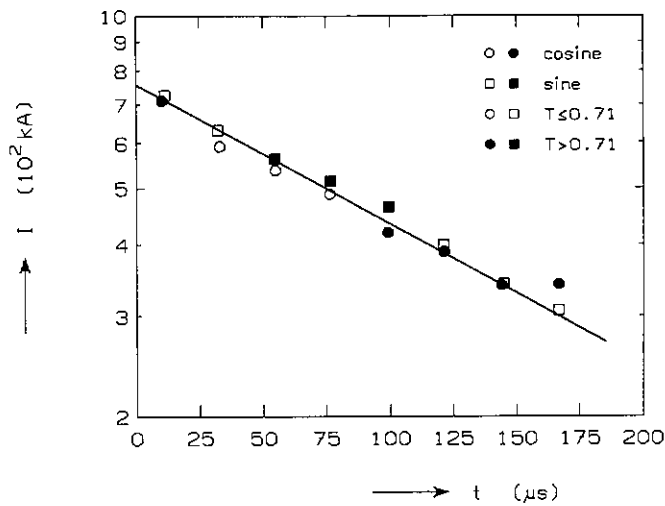


Fig. 7.6. The maxima and the minima of the current (calculated from Fig. 7.5), plotted logarithmically versus time.

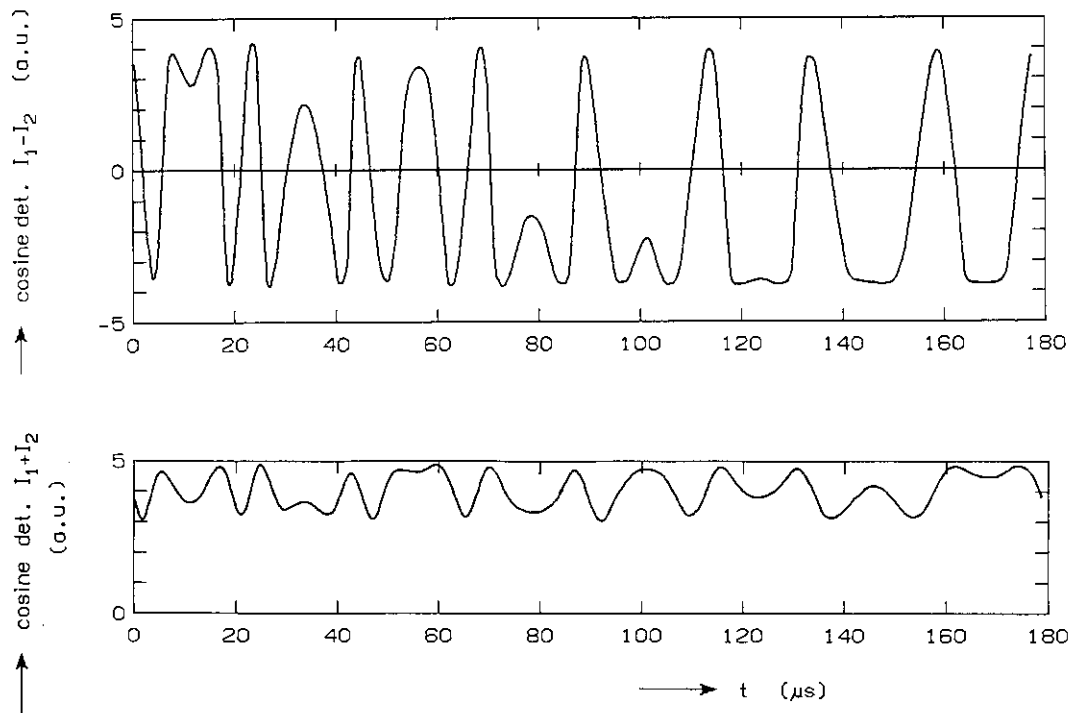


Fig. 7.7. I_2-I_2 and I_1+I_2 from the cosine-detector, recorded simultaneously. I_1+I_2 is not constant because of the beamsplitter.

In order to examine I versus time a measurement was carried out with I recorded only from the cosine detector. From this measurement a log-linear plot of the maxima and minima of the current was also made and this is shown in Fig. 7.8. From this plot it is obvious that the accuracy is much better now than in Fig. 7.6.

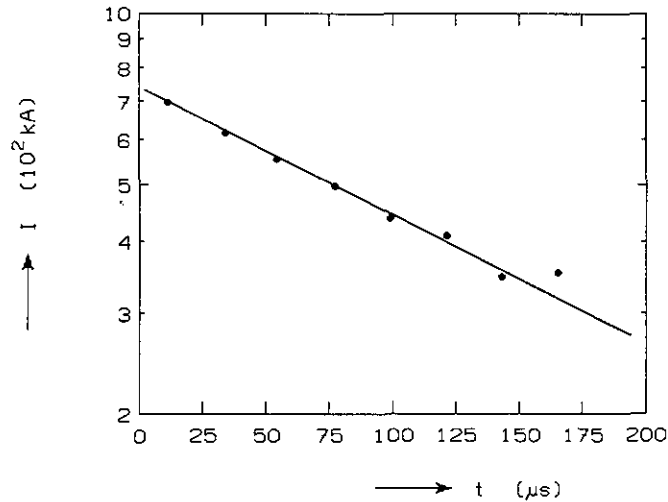


Fig. 7.8. Maxima and minima of the current calculated from the I-signal of the cosine-detector (with beamsplitter).

Apparently a proper calculation of the I-signal corrects to first order for the errors introduced by the beamsplitter prism.

7.3.3 Polarization properties of the beamsplitter prism

The intensity ($= I_1 + I_2$) of the light transmitted through the beamsplitter prism, is measured as a function of the angle of the plane of polarization; the result is shown in Fig. 7.9.

Figure 7.9 can be explained as follows:

One may regard the incoming plane polarized light as a superposition of two orthogonal polarizations. These two polarizations have different ratios of intensity of reflected light to intensity of transmitted light. As a consequence:

1. If the plane of polarization rotates, the intensity of the light leaving the beamsplitter is not a constant.
2. The angle of the plane of polarization after the beamsplitter prism is not the same as in front of the prism.

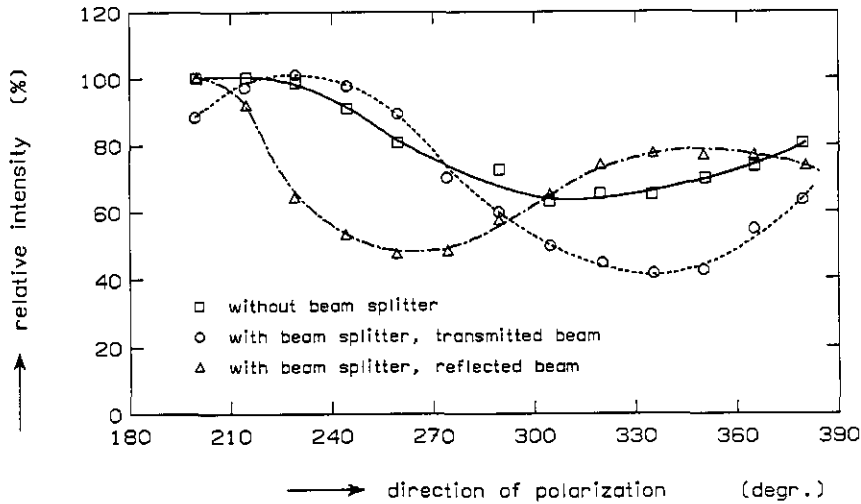


Fig. 7.9. Relative intensity of the two beams coming out the beamsplitter as a function of the angle of polarization. The intensity of the light without the beamsplitter prism is not a constant because the intensity of the light launched into the fiber depends on the angle of the direction of polarization.

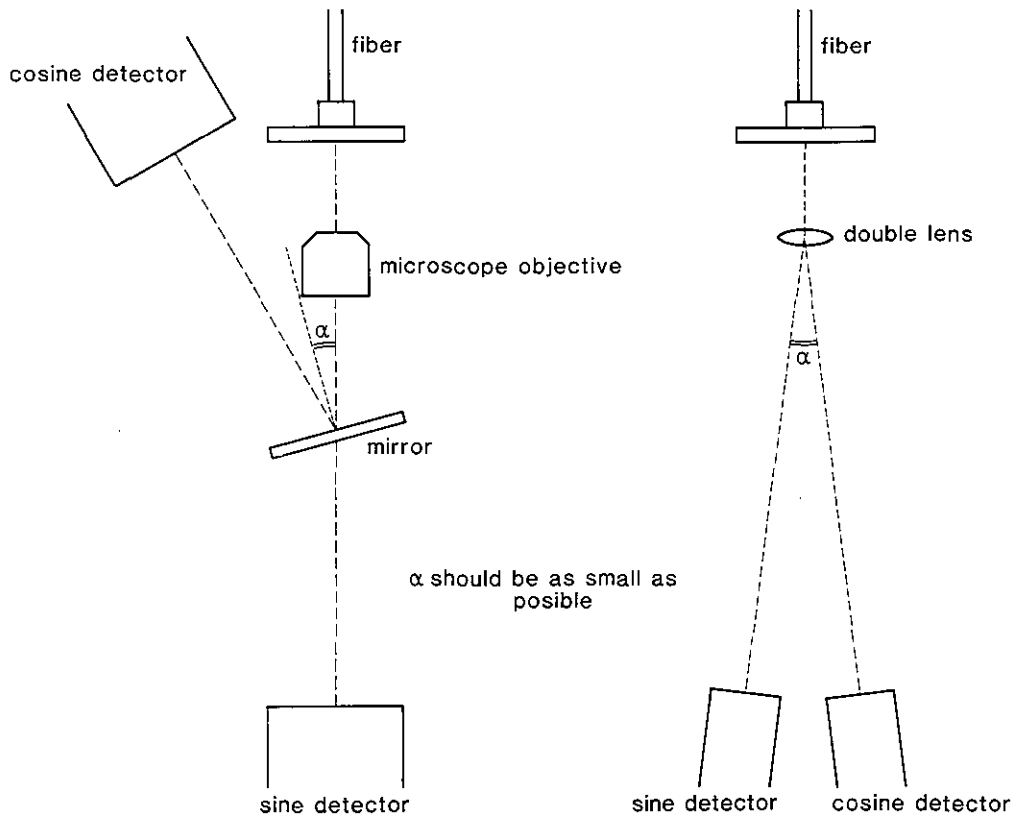
The last effect was also observed. If the detector is rotated such that $I = 0$ or 1 without beamsplitter prism and afterwards the beamsplitter prism is inserted, I is no longer 0 or 1 . However, the detector should not be rotated now, otherwise the signals will be asymmetrical (for positive and negative current).

7.4 Discussion

The results of the experiments show that a beamsplitter prism is not a proper instrument to build a double detector setup.

Since it is highly desirable to have a double detector system to avoid ambiguity, to gain in accuracy, and especially to make computer calculations of the current possible, a correct beamsplitter should be found.

Suitable components may be (1st) a 50% transparent mirror (Fig. 7.10) and (2nd) a double lens (Fig. 7.11).



Possible double detector setups:

Fig. 7.10.
With 50% transparent mirror.

Fig. 7.11.
With double lens.

8. CONCLUSIONS

In this report pulsed current measurements with a magneto-optic current meter are described.

First the optical properties of the spun single-mode fiber are examined and it is concluded that this type of fiber is quite suitable for use in a current meter. When the fiber is mounted, into the SPICA II experiment however, extreme care should be taken that along the whole length of the fiber no pressure is applied to the fiber; that the bending radius is not smaller than 15 cm, and that the parts of the fiber, which do not form part of the loop, are shielded against longitudinal magnetic fields.

Also the Verdet constant of this fiber has been measured, in order to calculate the current from the Faraday rotation: $V = 4.60 \times 10^{-6} \text{ rad A}^{-1}$.

In the pulsed experiments the optically measured current turned out to agree quite well with the current measured simultaneously with a Rogowski coil. The average error in the optical signal is about 1%. It is larger when the Faraday rotation ϑ is around the values $\pi/4$ and $3\pi/4$ rad ($I \approx 170$ and 510 kA resp.) and less when ϑ is more than $3\pi/4$ rad.

In order to calculate the current from the Faraday rotation with a computer program, a double detector is necessary. A setup with a beamsplitter prism and a double detector was constructed and several measurements were carried out. It is concluded that a beamsplitter prism is not the correct instrument for double detector measurements, but that double detector measurements are certainly possible when a proper beamsplitter is employed. A 50% transparent mirror and a double lens are suggested.

ACKNOWLEDGEMENTS

The author would like to thank Prof.Ir. P.C.I. van der Laan, Dr. A.A.M. Oomens and Dr.Ir. G.G. Wolzak for valuable discussions, the members of the high-voltage group of the electro-technical department of the Eindhoven University of Technology for their contributions to the investigations, Dr.Ir. W. van Etten (EUI) and W.J. Mastop (FOM) for their advice on fiber technology and the telecommunications group (of the EUI) for the use of their fiber equipment. In this report the results of the work carried out by R.J. Woltjer in 1982, were gratefully used.

This work was performed as part of the research programme of the association agreement of Euratom and the "Stichting voor Fundamenteel Onderzoek der Materie" (FOM) with financial support from the "Nederlandse Organisatie voor Zuiver-Wetenschappelijk Onderzoek" (ZWO), Euratom, and the "Stichting voor de Technische Wetenschappen" (STW).

REFERENCES

- [1] SPICA II-team; Prospects for SPICA II, Nucl. Instrum. & Methods 207 (1983) 61-73.
- [2] A.M. Smith; Optical fibers for current measurement applications, Optics and Lasertechnology, February 1980, p. 25-29.
- [3] A.M. Smith; Polarization and magneto-optic properties of single-mode optical fiber, Appl. Opt. 17 (1978) 52-56.
- [4] S.C. Rashleigh; Origins and control of polarization effects in single mode fibers, J. Lightwave Techn., LI-1, (1983) 312-331.
- [5] A.J. Barlow, J.J. Ramskov-Hansen and D.N. Payne; Birefringence and polarization mode-dispersion in spun single mode fibers, Appl. Opt. 20 (1981) 2962-2968.
- [6] A. Simon and R. Ulrich; Evolution of polarization along a single-mode fiber. Appl. Phys. Lett. 31 (1977) 517-520.
- [7] F.A. Jenkins and H.E. White; Fundamentals of optics, 3rd ed., McGraw-Hill, New York, 1957, 604-605.
- [8] R.C. Jones; A new calculus for the treatment of optical systems, J. Opt. Soc. Am. 31 (1941) 488-493.
- [9] R. Woltjer; Private communication, FOM I.R. 82/062.
- [10] W.J. Iabor and F.S. Chen; Electromagnetic propagation through materials possessing both Faraday rotation and birefringence: Experiments with Ytterbium Orthoferrite, J. Appl. Phys. 40 (1969) 2760-2765.
- [11] A.M. Smith; Birefringence induced by bends and twists in single-mode optical fiber, Appl. Opt. 19 (1980) 2606-2611.
- [12] G.I. Chandler and F.C. Jahoda; Proc. 10th Symp. on Fusion Engineering, Philadelphia (IEEE, New York, 1983), CAT. No. 83 cm 1916-6, 2084.

<u>CONTENTS</u>	<u>Page</u>
1. INTRODUCTION	2
1.1 Current measurements in SPICA II	2
1.2 The principle of the magneto-optic current-measurement	3
1.3 Demands on the optical fiber	4
2. DESCRIPTION OF THE TRANSMISSION OF PLANE POLARIZED LIGHT THROUGH A FIBER	7
2.1 A method to measure linear birefringence of a fiber	7
2.2 The measurement of a small linear birefringence	9
2.3 The optical signal of the current-meter if a fiber with linear birefringence is used	10
2.4 Current measurement with a "cosine detector"	12
3. EXPERIMENTAL APPARATUS	13
3.1 The light source	13
3.2 The fiber	14
3.3 The detecting part	14
4. PROPERTIES OF THE FIBER, USED IN THE EXPERIMENTS	16
4.1 Introduction	16
4.2 Intrinsic linear birefringence (δ_i)	16
4.3 Linear birefringence due to external mechanisms	17
4.3.1 Pressure	17
4.3.2 Bending	18
4.3.3 Mechanical vibrations	19
4.4 Conclusion	19
5. CALIBRATION	20
5.1 Introduction	20
5.2 The D.C.-current experimental setup	20
5.3 The adjustment of the current-meter	21
5.4 Results	21
5.5 Discussion	21

<u>CONTENTS</u>	<u>Page</u>
6. PULSED CURRENT MEASUREMENTS	24
6.1 Description of the experimental setup	24
6.1.1 The model	24
6.1.2 The current source	25
6.1.3 Miscellaneous equipment	26
6.2 Results	27
6.2.1 Current and optical signal versus time	27
6.2.2 Exponential decay and accuracy	27
6.2.3 Optical signal versus Rogowski signal (X-Y plots)	31
6.3 Discussion	33
7. DOUBLE DETECTOR MEASUREMENTS	34
7.1 Introduction	34
7.2 Experimental setup	36
7.3 Results	37
7.3.1 Optical signal versus time	37
7.3.2 Exponential decay; accuracy	38
7.3.3 Polarization properties of the beamsplitter prism	40
7.4 Discussion	41
8. CONCLUSIONS	43
ACKNOWLEDGEMENTS	43
REFERENCES	44
CONTENTS	45
APPENDIX	47

A P P E N D I X

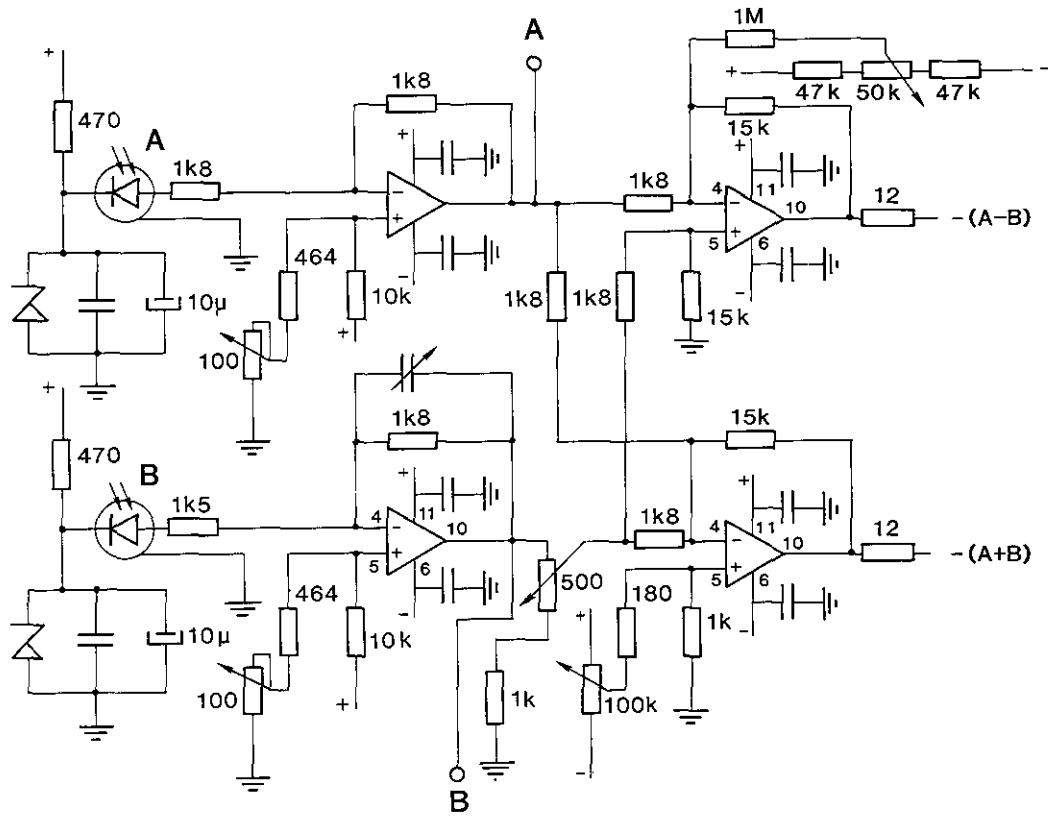


Fig. A1. Electronic circuit which calculates $I_2 - I_2$ and $I_1 + I_2$ (adder/subtractor), used in pulsed current measurements. Amplifier: HA5195, photodiode: MDA 435, power supply: ± 15 V, capacitor 10 nF, zener diode: BZX 85C (12 V).